Available online at www.sciencedirect.com
ScienceDirect
Trans. Nonferrous Met. Soc. China 33(2023) 3039−3053
Transactions of Nonferrous Metals Society of China
www.tnmsc.cn

Selective phase corrosion and cavitation erosion behaviors of various copper alloys in 3.5% NaCl solutions with different pH values

Qi-ning SONG[1], Hui-lin LI[1], Nan XU[1], Zhen-yu JIANG[1], Gen-yuan ZHANG[1], Ye-feng BAO[1], Yong-feng JIANG[1], Li-juan ZHAO[1], Cui-cui JI[1], Jian-hua ZHAO[1], Yan-xin QIAO[2]

1. College of Mechanical and Electrical Engineering, Hohai University, Changzhou 213022, China;
2. College of Materials Science and Engineering, Jiangsu University of Science and Technology, Zhenjiang 212003, China

Received 20 July 2022; accepted 15 February 2023

Abstract: The stability of each phase in nickel aluminum bronze (NAB), manganese aluminum bronze (MAB) and manganese brass (MB) was characterized by scanning Kelvin probe force microscopy (SKPFM). Selective phase corrosion (SPC) and cavitation erosion (CE) behaviors of these materials were studied in 3.5% NaCl solution with different pH values. The results show that the κ phase with the lowest stability is dissolved in the acidic solution (pH 2) for each material. In the neutral solution (pH 6.8), the Al-abundant κ phases in NAB are preserved, whereas the Fe-rich κ phases in MAB and MB are dissolved. In the alkaline solution (pH 12), pitting corrosion occurs at the κ phases in MAB and MB and at the κ_{II} phase in NAB. In each solution, NAB possesses the highest CE resistance, followed by MAB and MB. In the acidic solution, SPC remarkably intensifies the CE damage and CE−corrosion synergy contributes largely to the CE degradation. In other solutions, slight SPC occurs and each material exhibits a mechanical attack-dominated CE mechanism.

Key words: copper alloys; scanning Kelvin probe force microscopy; selective phase corrosion; cavitation erosion; synergy

1 Introduction

Ship plays an important role in guaranteeing security of the coastal defense and strengthening the marine trade. Propeller is the crucial propulsion device of a ship, and it suffers corrosion as a result of long-term immersion in seawater. When ship propeller rotates at a high speed, the liquid pressure fluctuates and cavitation occurs near the propeller blade. This causes the cavitation erosion (CE) damage on the propeller surface. Copper alloys, with high corrosion resistance and mechanical properties, are popularly applied as propeller materials [1]. Manganese brass (MB) has good workability but low strength, and it is prone to dezincification corrosion in seawater [2]. In contrast, manganese aluminum bronze (MAB) and nickel aluminum bronze (NAB), which are two typical Al bronzes with the addition of Ni, Fe and Mn, possess superior corrosion resistance, and they are primarily used for manufacturing large-sized and high-speed ship propellers [3,4]. These copper alloys generally have a multi-phase microstructure [4−6], and they are subjected to selective phase corrosion (SPC), because the difference in chemical composition and crystal structure among these phases give rise to galvanic corrosion [7−9]. These copper alloys exhibit different SPC behavior when the pH value or the species and concentration of aggressive ions in the corrosive media changes [10−12]. The adhesion of shellfish and accumulation of corrosion

Corresponding author: Qi-ning SONG, Tel: +86-519-85191938, Fax: +86-519-85120010, E-mail: qnsong@hhu.edu.cn
DOI: 10.1016/S1003-6326(23)66316-2

products on the ship propellers creates the crevice environments, where the solution is acidized and enriched with aggressive ions. The presence of some pollutants alters pH value in seawater [12]. Sulfide, which is a common pollutant induced by industrial waste discharge, can significantly reduce the corrosion resistance of copper alloys [13,14], and it makes the surrounding seawater alkaline.

The SPC behavior of copper alloys has attracted the attention of many researchers. It was reported that the α phase in the eutectoid microstructure $\alpha+\kappa_{III}$ of the NAB was preferentially corroded and the κ_{II} phase was well preserved in the neutral chloride solution [7,10,12]. LV et al [15] found that after short-period immersion in 3.5% NaCl solution, the κ_{II} phase in the cast NAB exhibited lower conductivity as a result of the rapid formation of an Al_2O_3 film, compared with the α matrix. However, the κ_{II} phase in the cast NAB was preferentially dissolved when the pH value of the chloride solution was lower than 4.0 [10]. NAKHAIE et al [16] applied scanning Kelvin probe force microscope (SKPFM) to evaluate the nobilities of different phases in the NAB, and found that the κ phase with low nobility was preferentially corroded in 0.1 mol/L HCl solution. However, the SPC behavior of the NAB in the alkaline solution has been lack of investigation. Besides, the MAB is also subjected to SPC. It was reported that the κ phase with high Fe and Mn contents was found to be dissolved preferentially in 3.5% NaCl solution [8,17,18]. However, how SPC behavior of the cast MAB and MB changes with the pH value has been rarely reported. Furthermore, CE and corrosion work synergistically on the ship propeller [19,20]. The occurrence of SPC is expected to aggravate the CE damage of these multi-phase copper alloys. It was reported that SPC at the eutectoid microstructure $\alpha+\kappa_{III}$ and β' phases of the cast NAB induced a considerable CE-corrosion synergy, which contributed to over 30% of the cumulative CE mass loss in 3.5% NaCl solution [13,21]. However, the CE behavior of these copper alloys in the chloride solution with different pH values has been lack of research, and the effect of SPC on the CE behavior is also unclear.

In the present study, the nobility of various phases in the cast MAB, NAB and MB were characterized by SKPFM. Corrosion morphologies of different phases were observed to recognize the SPC behavior of these copper alloys after immersion in 3.5% NaCl solutions with different pH values. CE mass loss measurement, surface morphologies observation and electrochemical tests were performed to characterize the CE behavior. The SPC mechanism and its effect on the CE behavior of these copper alloys were discussed.

2 Experimental

2.1 Materials and test solutions

The investigated materials were three cast copper alloys, namely MAB, NAB and MB. The chemical composition is listed in Table 1. Analytical sodium chloride and distilled water were used to prepare 3.5% NaCl solution (its pH value is nearly 6.8), which was noted as the neutral solution hereinafter. Hydrochloric acid or sodium hydroxide was added in 3.5% NaCl solution to adjust the pH value.

Table 1 Chemical composition of three copper alloys (wt.%)

Alloy	Al	Ni	Fe	Mn	Cu	Zn
NAB	9.18	4.49	4.06	1.03	Bal.	−
MAB	7.28	2.10	3.62	12.35	Bal.	−
MB	0.86	0.22	0.89	2.17	55.70	Bal.

2.2 SKPFM measurements

SKPFM measurements were carried out using a scanning probe microscope (SPM) system (Bruker Corporation, Dimension Icon) at room temperature with a relative humidity of (20±5)%. The tip was a magnetic etched silicon probe (HQ:NSC18/Pt, Brock Company, USA) with a length of (220−230) μm, and it worked at a resonant frequency of (60−90) kHz. Dual scan mode was adopted. The surface topography signal was obtained in a tapping mode during the first scan. During the second scan, an oscillating alternating current (AC) potential was applied to the tip to cause a simple resonant swing, and the tip was raised 50 nm to obtain the voltammetry potential signal. In order to balance the contact potential difference (V_{cpd}) between tip and sample, a direct current (DC) bias potential was applied to the tip of the probe during scanning. The bias potential was obtained from $V_{cpd}=(\phi_{tip}-\phi_{sample})/e$, and denoted as Volta potential (VP) in this study, where e was the

value of charge, and ϕ_{tip} and ϕ_{sample} were the work functions of the tip and sample, respectively. In this measurement, the value of ϕ_{tip} was constant, and ϕ_{sample} represented the minimum energy required for electrons to escape from the solid surface. The lower work function of the material generally corresponded to the higher corrosion tendency [22]. In the VP map, the high-potential region had lower electrochemical nobility and higher corrosion tendency.

Before the SKPFM measurements, the tested sample was mechanically ground with abrasive papers up to 5000 grits, then polished to 0.5 μm using diamond paste and finally polished to 0.02 μm using colloidal suspension. At least three different regions were selected in order to ensure the repeatability.

2.3 Corrosion tests

Three copper alloys were mechanically polished and immersed in different solutions, and the surface morphologies were observed by scanning electron microscopy (SEM, JEOL JSM−6360LA) to figure out the SPC behavior. The chemical composition of the corroded surface was measured by energy dispersive spectroscopy (EDS, Oxford X-MAX20). The electrochemical measurements were performed in different solutions with a Gamry Interface 1000E potentiostat using a typical three-electrode system. The samples were sealed with epoxy resin with an exposed surface of 10 mm × 10 mm and used as working electrodes. The counter and reference electrodes were a platinum plate and a saturated calomel electrode (SCE), respectively. The sample was firstly immersed in the test solution for about 1800 s to obtain a stable open circuit potential (OCP), and then the polarization curves were recorded at a scanning rate of 0.5 mV/s in the potential range from −0.5 to 1.3 V versus the OCP. Electrochemical impedance spectroscopy (EIS) was performed at the OCP in a frequency range from 10^5 to 10^{-2} Hz with an oscillation voltage amplitude of 5 mV.

2.4 CE tests

The CE test was carried out using an ultrasonic vibration device according to the ASTM G32—2010 [23]. The sample was weighed using an electronic balance with a precision of 0.1 mg, and then it was placed 0.5 mm right below the ultrasonic probe. The upper surface of the sample was 15 mm below the liquid surface. The amplitude of the horn was 60 μm and the vibration frequency was 20 kHz. The sample was weighed at different intervals and the test duration was 5 h. The temperature of the test solution was kept at 18−22 °C by circulating cooling water. The mean depth of erosion (MDE, D_E) was obtained using Eq. (1):

$$D_E=\Delta m/(\rho\cdot S) \quad (1)$$

where Δm is the CE mass loss, ρ is the density of the copper alloys and S is the working area of sample. The electrochemical measurements under the CE condition were realized by connecting the ultrasonic vibration device with the potentiostat. The OCP of the test sample under alternating quiescence and CE conditions was recorded, and each condition lasted for 1800 s. The potentiodynamic polarization was also performed under CE condition and the results were analyzed by CView 3.2 software. The surface morphologies of the eroded samples were observed by SEM. All the electrochemical and CE tests were conducted in triplicate. The results were reproducible and represented the average level.

3 Results

3.1 SKPFM results

The microstructure, VP map and line scan profile of three copper alloys are shown in Fig. 1. The lighter region in the VP map has higher VP and correspondingly lower nobility. The VP difference among different phases can be obtained from the line scan profiles. The MAB consists of the α matrix, irregularly shaped β and rosette κ phases (Fig. 1(a)). The κ phase has the highest VP, followed by β and α. The VP values of κ and β phases are approximately 50 and 15 mV higher than that of the α phase, respectively (Figs. 1(b, c)). The NAB is composed of the α matrix, retained β' and various κ phases, including the fine κ_{IV} phase inside the α matrix, the κ_{II} phase along the α phase boundaries and the lamellar κ_{III} phase in the eutectoid microstructure (Fig. 1(d)). The VP value orders from high to low as κ_{II}, κ_{III}, κ_{IV}, and α. VP difference reaches 80 mV between α matrix and κ_{II}, and 25 mV between α matrix and κ_{IV}. In the

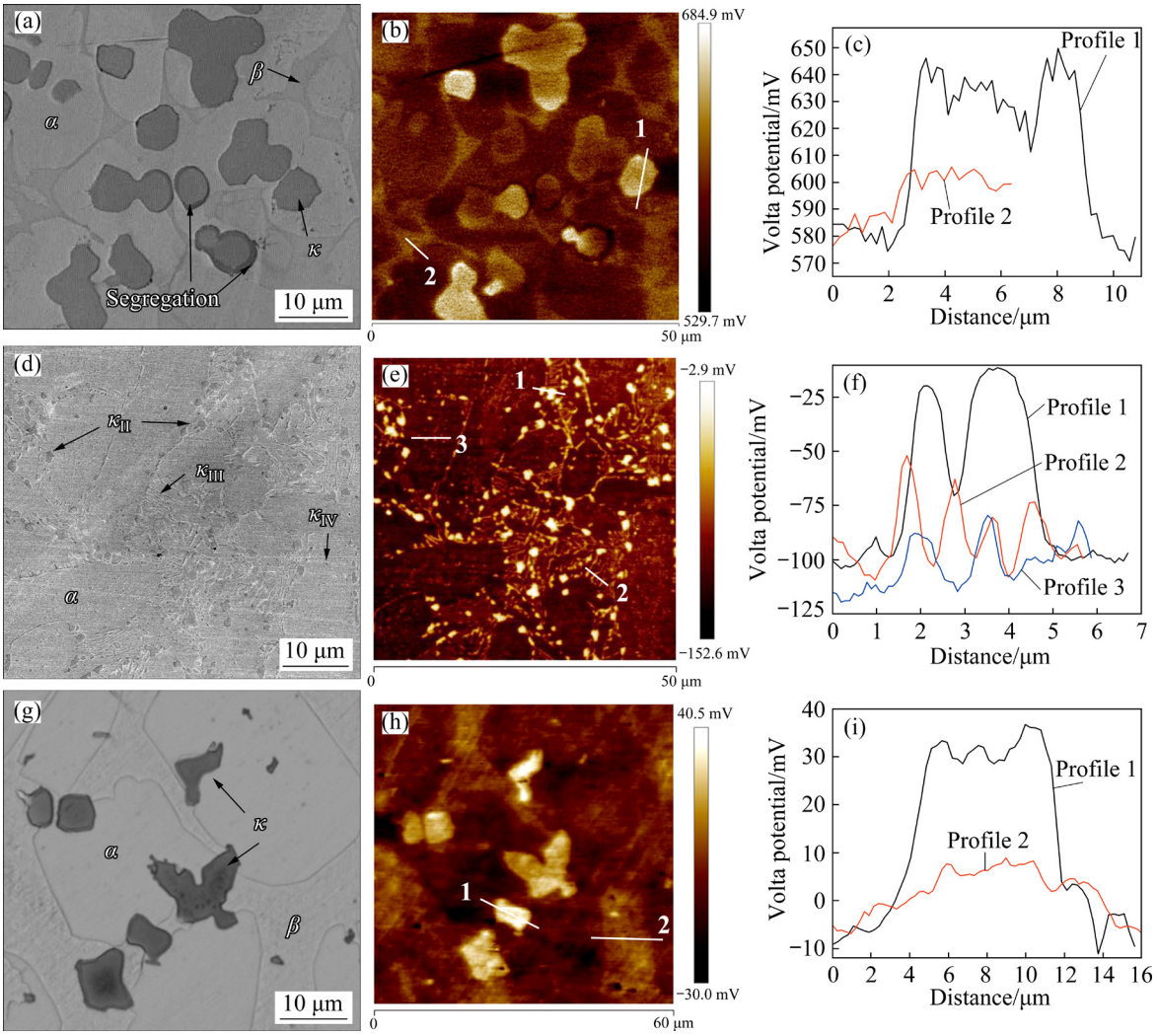

Fig. 1 Microstructure (a, d, g), VP maps (b, e, h) and line scan profiles (c, f, i) of MAB (a−c), NAB (d−f) and MB (g−i)

eutectoid microstructure, VP difference between the α and κ_{III} is up to 50 mV, as shown in Figs. 1(e, f). The MB consists of the β matrix, coarse α and κ phases, which are mainly distributed inside the α phases and at the α/β phase boundaries (Fig. 1(g)). The κ phase has the highest VP, which is 25 mV higher than that of β phase, and 35 mV higher than that of α phase, as indicated in Figs. 1(h, i).

The VP of each phase in the material was highly related to the work function of the involved elements [24−26]. The chemical composition results of each phase in the three copper alloys obtained by EDS are listed in Table 2. For MAB, the κ phase contains a high content of Fe (66%), which possesses lower work function than Cu [22]. Therefore, the α and β phases, which are Cu-rich solid solutions [5], have lower VP values than the κ phase. The β phase has higher Al and Mn contents but a lower Cu content. Correspondingly, it has a higher VP and a lower nobility than the α phase. PUNBURI et al [18] also reported that the α phase possesses the highest work function, followed by the β and κ phases in a Cu−8Mn−8Al alloy. For the NAB (Figs. 1(d, e)), the κ_{II} phase is a Fe_3Al-based intermetallic compound [5]. It has the highest Fe content and also a high Al content. Therefore, it has the highest VP and the lowest nobility. The κ_{IV} phase has a similar chemical composition and crystal structure with κ_{II} [5], but it exhibits a lower VP, because it is much smaller in size and its VP result is influenced by the surrounding α matrix with a lower VP [11]. The κ_{III} phase is a NiAl-based intermetallic compound with a Ni content approaching 30% [5], and Ni has a higher work function than Fe [22]. As a result, κ_{III} exhibits a lower VP and it is nobler than κ_{II}. For the MB

(Figs. 1(h, i)), the β phase has a higher VP and a lower nobility than the α phase, because it possesses higher contents of Al, Mn and Zn with low work function [22]. CHEN et al [27] also reported a similar SKPFM result that the β phase exhibits a lower work function than the α phase in a H62 brass. The κ phase has the highest VP and the lowest nobility, because it contains the highest Fe content (exceeding 80%).

Table 2 Chemical compositions of different phases in three copper alloys (wt.%)

Material	Phase	Al	Ni	Fe	Mn	Cu	Zn
MAB	α	5.70	3.00	4.20	11.60	75.50	–
	β	9.46	3.22	1.80	14.74	70.78	–
	κ	5.80	1.80	66.00	14.50	11.90	–
NAB	α	7.62	3.49	3.40	0.88	84.61	–
	β'	9.70	5.26	2.20	1.07	81.77	–
	κ_{II}	13.07	11.08	60.45	1.74	13.66	–
	κ_{III} [5]	22±4	28±5	22±5	1.6±0.4	26±4	–
	κ_{IV} [5]	9±4	6±4	60±8	1.6±0.4	23±6	–
MB	α	0.61	0.37	0.22	2.05	62.60	34.15
	β	0.99	0.33	0.18	2.58	56.24	39.68
	κ	4.33	0.25	86.06	4.62	2.86	1.88

3.2 Electrochemical test results and SPC morphologies

Figure 2 shows the polarization curves of the three copper alloys in different solutions. Each material exhibits the lowest corrosion potential (φ_{corr}) and the largest current density (J_{corr}) in the solution of pH 2, but the highest potential in the solution of pH 12. Besides, an obvious passive region appears in the anodic branch of the polarization curves and all the three copper alloys exhibit a passive behavior in the alkaline solution. The MAB has the lowest pitting potential, and the current density gradually increases with the applied potential in the passive region, indicating the inferior passive ability. The passive current density of the MB is nearly one order of magnitude lower than that of the MAB and NAB. Figure 3 shows the EIS results of different copper alloys. For both the NAB and MB, the impedance in the solution of pH 12 is much higher than that in the other two solutions. This evidences that the passive films can be rapidly built on these two copper alloys and the MB has the most protective passive film in the solution of pH 12. However, the MAB has a much lower impedance than the other two copper alloys. This indicates that an intact passive film cannot be built after such a short immersion period (about 1800 s) in the solution of pH 12, or the passive film is poorly protective for the MAB.

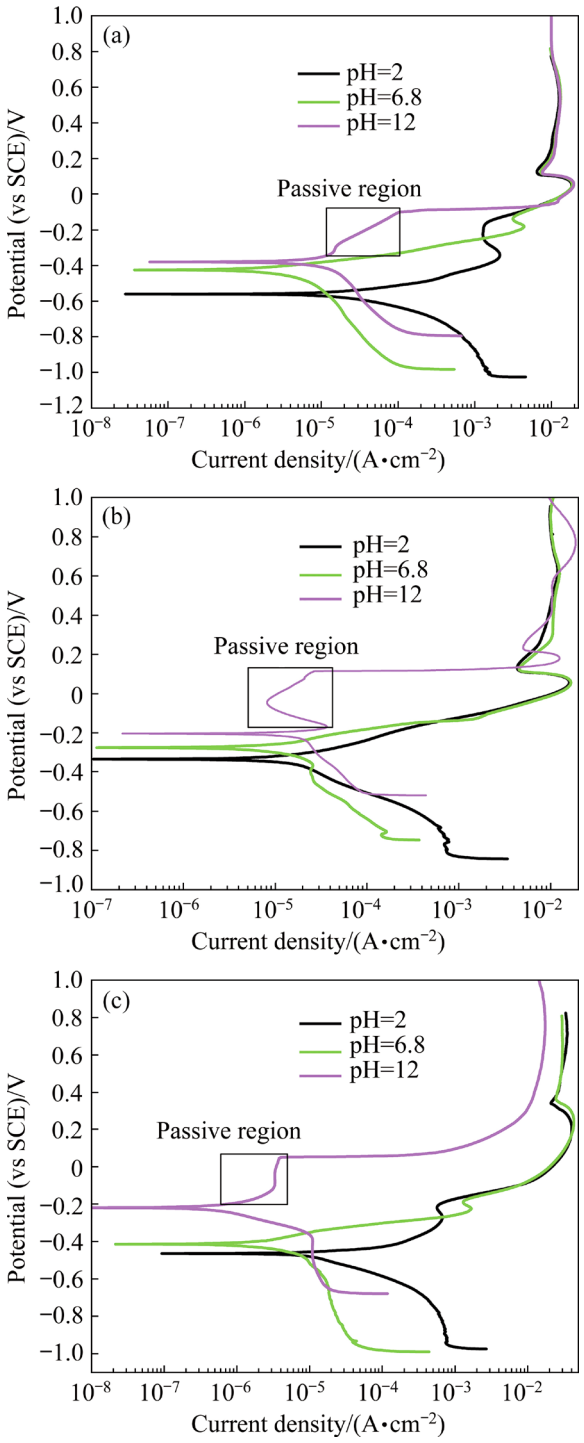

Fig. 2 Potentiodynamic polarization curves of MAB (a), NAB (b) and MB (c) in 3.5% NaCl solution with different pH values

Figure 4 shows the surface morphologies of the three copper alloys after immersion in different solutions for 6 h. For the MAB, severe dissolution of the rosette κ phases occurs in the solution of pH 2 (Fig. 4(a)). Only some of the κ phases are dissolved and the β phases suffer preferential corrosion in the neutral solution (Fig. 4(b)). In the solution of pH 12, small corrosion pits appear at the κ phases and both the α and β phases are covered by corrosion products (Fig. 4(c)). In the solution of pH 2, Fe, Mn and Al are actively dissolved. The VP result also shows that the κ phase exhibits the lowest nobility and correspondingly the highest corrosion tendency. Therefore, the κ phase is dissolved rapidly. As reported previously, segregation occurs at the periphery of the large-sized rosette κ phases, and this creates galvanic corrosion [17]. Preferential corrosion occurs at the segregation region and extends into the center of the κ phase in the neutral solution. TRETHEWEY et al [28] also found that the dissolution of the κ phases gives rise to the generation of brown rusts of Fe and Mn oxides on the surface in seawater. Afterwards, corrosion proceeds in the manner of other α+β bronzes, and preferential attack occurs at the β phase. It was reported that the presence of a low concentration of Mn oxides hampers the formation of a compact film on Cu−Al−Mn alloy

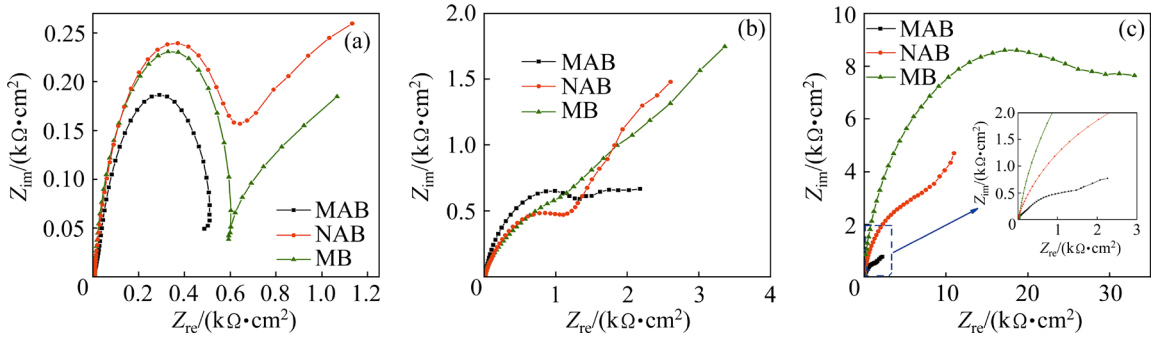

Fig. 3 Nyquist plots of three copper alloys after 30 min immersion in 3.5% NaCl solution of pH 2 (a), pH 6.8 (b) and pH 12 (c)

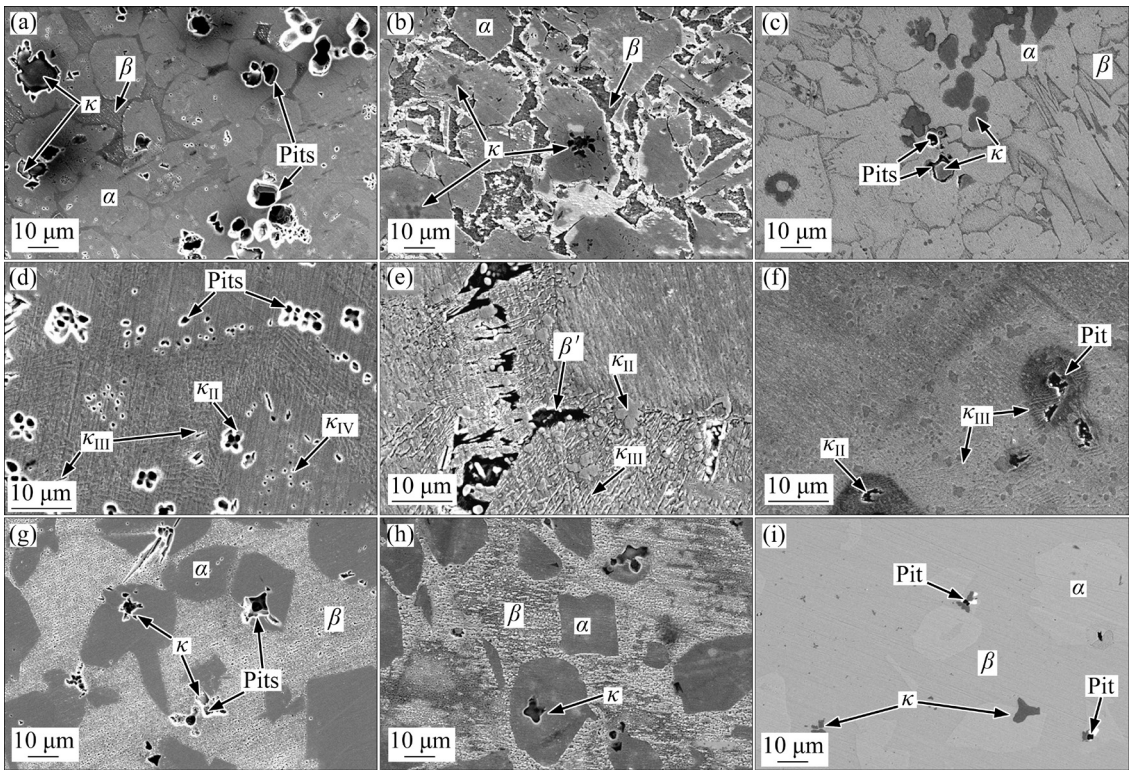

Fig. 4 Surface morphologies of MAB (a−c), NAB (d−f) and MB (g−i) after immersion in 3.5% NaCl solution with different pH values: (a, d, g) pH 2; (b, e, h) pH 6.8; (c, f, i) pH 12

in 3.5% NaCl solution [29]. Thus, the poorly-protective film is also responsible for the preferential dissolution of the κ phase in the neutral solution. In the solution of pH 12, a passive film can be built on the surface, but the film is considered poorly protective, as indicated in Figs. 2(a) and 3(c). Moreover, the film is inhomogeneous, with the α and β phases covered by copper oxides and the κ phases covered by poorly protective Fe and Mn oxides [30]. Therefore, corrosion pits are prone to generate at these κ phases.

For the NAB, the κ_{II} and κ_{IV} phases are completely dissolved, whereas only a fraction of κ_{III} are subjected to dissolution in the solution of pH 2 (Fig. 4(d)). In the neutral solution, severe corrosion occurs at the β' phases, but the κ_{II} phase is scarcely dissolved. In the eutectoid microstructure, the lamellar α phase undergoes preferential corrosion and the κ_{III} phase is remained (Fig. 4(e)). In the solution of pH 12, corrosion pits appear as a result of the dissolution of some κ_{II} phases, whereas no obvious corrosion is found at the eutectoid microstructure (Fig. 4(f)). As generally reported, the Al-abundant κ phases act as cathodes in the neutral chloride-containing solution, because a protective Al_2O_3 film is built on them [15]. It was also reported that the κ phases in the Fe, Ni-containing Al bronze are in a passive state in 3% NaCl solution [31]. The β' phase is also preferentially corroded, because it exhibits an unstable martensite structure with many small precipitates inside and this leads to galvanic corrosion [7]. However, a stable Al_2O_3 film can not exist in the solution with the pH value lower than 4.0, and the κ phases with low nobilities are dissolved [10,12], as also reported in our previous study [11]. In the alkaline solution with the pH value lower than 9.5, the oxidation of Al atoms leads to the formation of protective Al_2O_3 through Eq. (2):

$$2Al+6OH^-\rightarrow Al_2O_3\cdot xH_2O+(3-x)H_2O+6e \quad (2)$$

When the pH value exceeds 10, the Al_2O_3 transforms into aluminates (AlO_2^-), which is soluble in the aqueous solution [32]:

$$Al_2O_3+2OH^-\rightarrow 2AlO_2^-+H_2O \quad (3)$$

However, the Cu atoms are more easily oxidized by hydroxide ions to form a more compact passive film structure through Eq. (4) [32,33]:

$$2Cu+2OH^-\rightarrow Cu_2O+H_2O+2e \quad (4)$$

Therefore, a passive film, with copper oxides as the main component, is expected to be generated on the NAB, notwithstanding the absence of the Al_2O_3. Pitting corrosion mainly occurs at the κ_{II} phases, probably due to the active dissolution of Al and the inferior protectiveness of Fe oxides.

For the MB, the κ phases with the lowest nobility are completely dissolved and the β phase is also severely corroded in the solution of pH 2 (Fig. 4(g)). The β phase undergoes pretty severe dezincification corrosion and its Zn content plunges from approximately 40% to 10%, based on the EDS result (not presented here). In the neutral solution, a large number of κ phases are dissolved and severe corrosion also occurs at the β phase (Fig. 4(h)). The β phase also suffers dezincification corrosion, and its Zn content falls from approximately 40% to 25%. It was reported that the redeposition of Cu occurs in the dezincification process of brass [26,34], and the spongy deposited Cu can act as the cathodes and further facilitate the active dissolution of the κ phases. In the solution of pH 12, very slight corrosion occurs on the MB (Fig. 4(i)). It was reported that the Cu−Zn alloys exhibit a passive behavior and high corrosion resistance in the alkaline solution, owing to the generation of the Cu and Zn oxides on the surface [35,36], as also indicated in Fig. 2(c). A small quantity of the Fe-rich κ phases undergo pitting corrosion, as the κ_{II} phases of the NAB and the κ phases of the MAB behave in the solution of pH 12.

As indicated above, there hardly exists a monotonous relationship between the VP results and practical corrosion behavior. In the acidic solution, the alloying elements in the three copper alloys are actively dissolved as: $M\rightarrow M^{n+}+ne$ (M could be Fe, Al, Zn and Mn), and there is no passive film built on the surface. Therefore, preferential corrosion is prone to occur at the phases with low nobilities and the VP results are reliable to evaluate the corrosion tendency of different phases. However, the VP result, which is merely obtained in air, should be handled cautiously if corrosion product films are generated on the surface of these copper alloys after immersion in the test solutions. In the neutral and alkaline solutions, the alloying elements of these copper alloys can be passivated through the formation of stable oxides or hydroxides, and thus

the corrosion process is inhibited. Corrosion preferentially occurs at the sites, where the film is defective and poorly protective. Other researchers also proposed that VP results obtained by SKPFM cannot be universally correlated with practical corrosion behavior in a certain solution [25,26].

3.3 MDE results and CE morphologies

Figure 5 shows the MDE results of the three copper alloys after CE for 5 h in different solutions (the density is 7.4793, 7.4093 and 8.1610 g/cm^3 for the NAB, MAB and MB, respectively). It is found that the MB has the highest MDE, followed by the MAB and NAB in each solution. Each material has the highest MDE in the solution of pH 2, and the lowest MDE in the solution of pH 12. For the MB, the MDE in the acidic solution reaches 6.97 μm, which is 1.74 and 1.92 times larger than that in the neutral and alkaline solutions, respectively. For the MAB, the MDE in the acidic solution is up to 3.88 μm, which is 1.75 and 2.55 times larger than that in the neutral and alkaline solutions, respectively. This indicates that both the MB and MAB are subjected to much more severe corrosion in the acidic corrosion. In contrast, the corrosion damage of the NAB increases moderately with decreasing the pH value. The MDE of the NAB in the acidic solution is only 1.58 μm, which is 0.66 times larger than that in the neutral solution and 1.22 times larger than that in the alkaline solution.

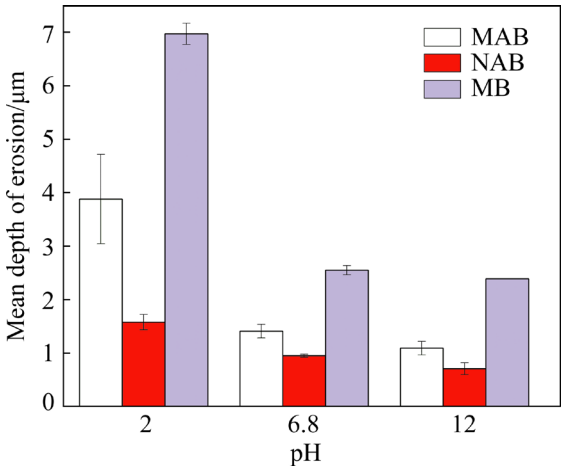

Fig. 5 MDE results of three copper alloys after CE for 5 h in 3.5% NaCl solution with different pH values

Figure 6 shows the surface morphologies of the three copper alloys after CE in different solutions for 1 h. It is obvious that much more severe CE damage occurs in the solution of pH 2, and the dissolution of these κ phases results in the

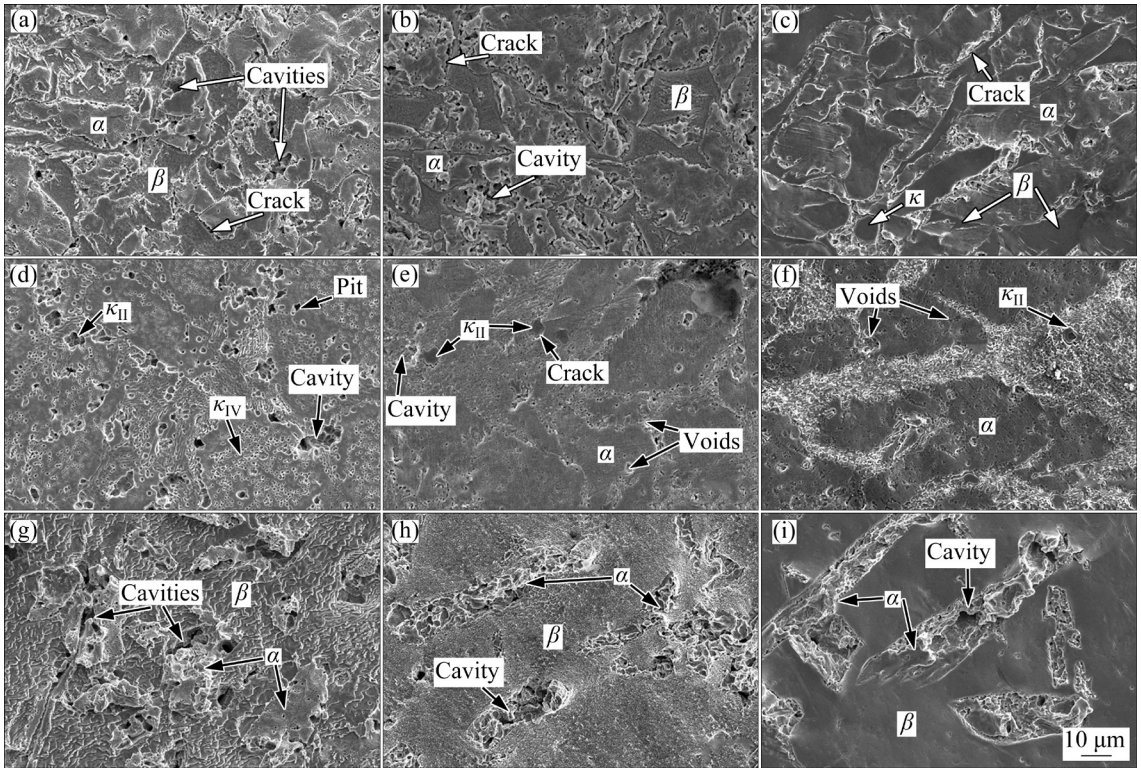

Fig. 6 Surface morphologies of MAB (a−c), NAB (d−f) and MB (g−i) after CE for 1 h in 3.5% NaCl solution of pH 2 (a, d, g), pH 6.8 (b, e, h) and pH 12 (c, f, i)

generation of corrosion pits for each copper alloy, as shown in Figs. 6(a, d, g). For the MAB, cracks appear at the α/β phase boundaries, and obvious deformation and voids are found at the α phases in each solution. The β phase undergoes preferential corrosion in both the acidic and neutral solution (Figs. 6(a, b)), but it is hardly corroded in the solution of pH 12 (Fig. 6(c)). For the NAB, the corrosion pits extend under the cavitation stress, leading to the generation of large cavities in the solution of pH 2 (Fig. 6(d)). In the neutral solution, cracks appear at the α/κ_{II} boundaries, and small voids distribute at the periphery and interval of the α matrix. Besides, cavities are also found at the eutectoid microstructure (Fig. 6(e)). In the solution of pH 12, the eutectoid microstructure and β' phases are subjected to preferential corrosion. Voids are found inside the α matrix and cracks appear at the α/κ_{II} phase boundaries (Fig. 6(f)). For the MB, the α phase is severely attacked, resulting in the appearance of many cavities and obvious material detachment in each solution. In the solution of pH 2, distinct undulation is found at the β phase as a result of severe corrosion, and few original microstructures are left on the surface (Fig. 6(g)). The β phases also suffer relatively slight corrosion in the neutral solution (Fig. 6(h)), but they are scarcely corroded in the solution of pH 12 (Fig. 6(i)).

The surface morphologies of the three copper alloys after CE for 5 h are presented in Fig. 7. Obvious cavities appear on the surface of each material, and the original microstructure can be hardly distinguished. For the MAB, the β phase is lower in height than the surrounding α phase due to the preferential corrosion in the solution of pH 2. Besides, there are also some holes and pits on the surface, probably because of the dissolution of the κ phases (Fig. 7(a)). In both the neutral and alkaline solutions, the β phase suffers brittle fracture and the debris of β phase protrudes on the surface (Figs. 7(b, c)). For the NAB, many pits and cavities are distributed on the surface in the solution of pH 2 (Fig. 7(d)). Groove-shaped cavities appear as a result of the material detachment in both the neutral and alkaline solutions (Figs. 7(e, f)). The debris of the eutectoid microstructure is visible on the surface in the neutral solution (Fig. 7(e)). For the MB, the β phases are subjected to extremely severe corrosion, and this makes the surface undulating in the solution of pH 2. Moreover, the α phase protrudes on the surface as a result of the corrosion of the

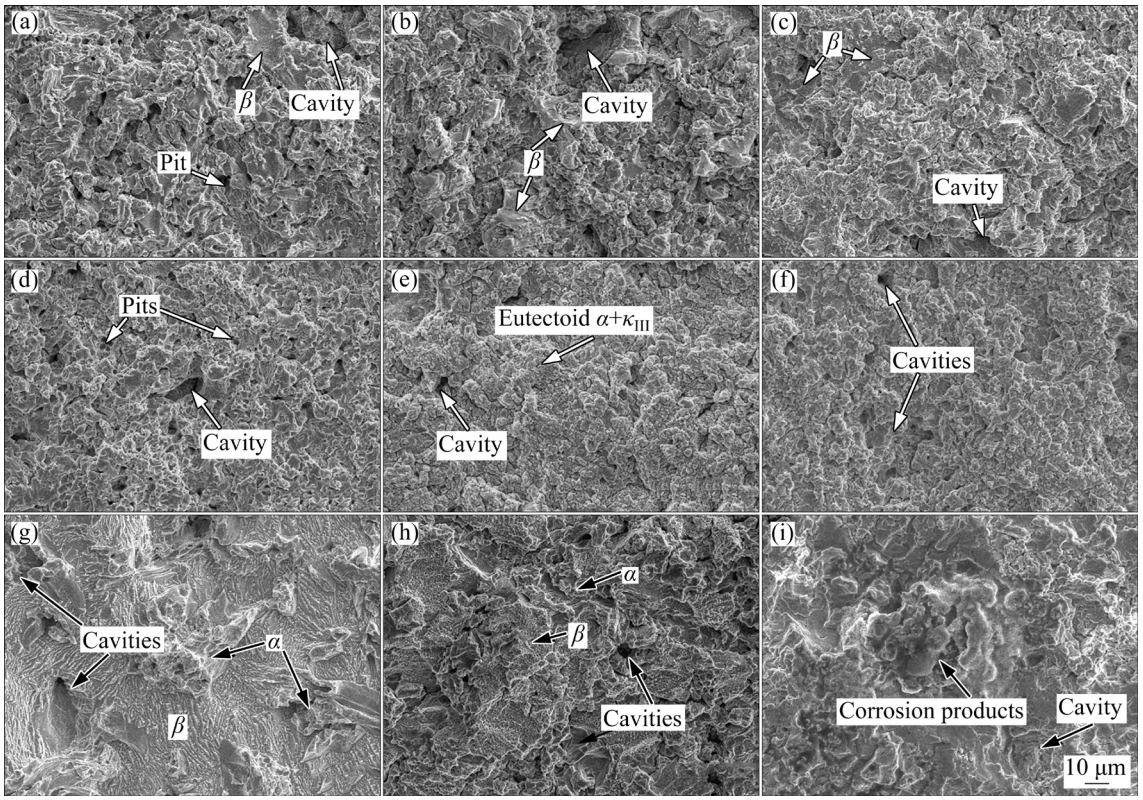

Fig. 7 Surface morphologies of MAB (a−c), NAB (d−f) and MB (g−i) after CE for 5 h in 3.5% NaCl solution of pH 2 (a, d, g), pH 6.8 (b, e, h) and pH 12 (c, f, i)

surrounding β matrix (Fig. 7(g)). In the neutral solution, preferential corrosion also occurs at the β phases, and groove-shaped cavities appear on account of the erosion damage at the α phases (Fig. 7(h)). In the solution of pH 12, the surface is much more mildly attacked. Besides, thick corrosion products are locally found on the surface (Fig. 7(i)).

3.4 Electrochemical behavior under CE condition

Figure 8 shows the OCP results of the three copper alloys under alternating quiescence and CE conditions in different solutions. For the MAB, the OCP shifts to a more positive value when CE starts, but it decreases once CE is terminated in each solution (Fig. 8(a)). For the NAB, CE causes a positive OCP shift in the solution of pH 2, but a negative OCP shift in other solutions (Fig. 8(b)). For the MB, CE shifts the OCP to a more negative value in the solution of pH 12, whereas a more positive value in other solutions (Fig. 8(c)). Figure 9 shows the polarization curves of the three copper alloys in different solutions under the CE condition, and Table 3 presents the φ_{corr} and J_{corr}

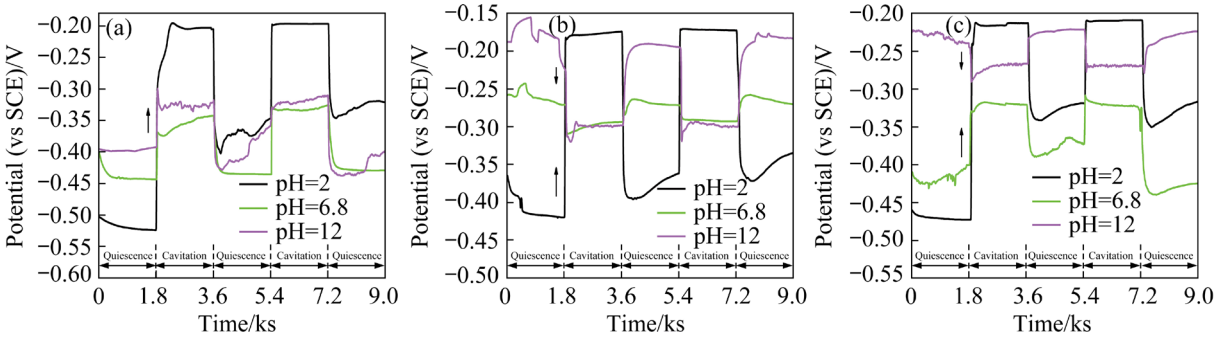

Fig. 8 OCP results of MAB (a), NAB (b) and MB (c) in 3.5% NaCl solution with different pH values under alternate conditions of quiescence and CE

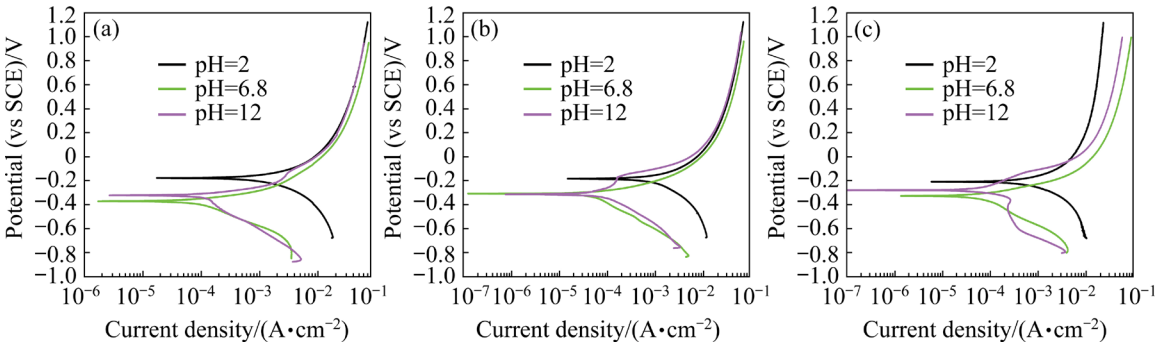

Fig. 9 Potentiodynamic polarization curves of MAB (a), NAB (b) and MB (c) under CE condition in 3.5% NaCl solution with different pH values

Table 3 Electrochemical parameters obtained from polarization curves for copper alloys in 3.5% NaCl solutions with different pH values

Material	Condition	J_{corr}/(A·cm^{-2})			φ_{corr}(vs SCE)/mV		
		pH=2	pH=6.8	pH=12	pH=2	pH=6.8	pH=12
MAB	Quiescence	3.320×10^{-5}	7.458×10^{-6}	1.211×10^{-5}	−562	−422	−379
	CE	9.322×10^{-4}	8.513×10^{-5}	8.998×10^{-5}	−174	−372	−325
NAB	Quiescence	1.070×10^{-5}	4.396×10^{-6}	8.354×10^{-6}	−338	−276	−207
	CE	6.086×10^{-4}	5.322×10^{-5}	8.012×10^{-5}	−187	−311	−313
MB	Quiescence	1.180×10^{-5}	8.096×10^{-6}	4.096×10^{-7}	−463	−416	−216
	CE	8.476×10^{-4}	7.621×10^{-5}	7.000×10^{-5}	−205	−325	−276

results obtained from Figs. 2 and 9. It is found that in each solution, CE significantly increases the J_{corr} of each copper alloy, compared with the result under the quiescence condition.

When the material is covered by a protective corrosion product film or a passive film under the quiescence condition, CE destroys the film and consequently causes a negative OCP shift. If the material undergoes active dissolution or the film protectiveness is poor, CE primarily expedites the cathodic process by accelerating the mass transfer in solution (mainly the dissolved oxygen), and causes a positive OCP shift [37,38]. In the solution of pH 2, no films are built on the three copper alloys. The cathodic process consists of hydrogen evolution and oxygen reduction:

$$2H^{+}+2e\rightarrow H_2 \quad (5)$$

$$O_2+4H^{+}+4e\rightarrow 2H_2O \quad (6)$$

The OCP of each copper alloy is raised by CE as a result of the accelerated oxygen transfer in the solution. Due to the dissolution of these κ phases, the remaining surface of each copper alloy is depleted in Fe, Mn and Al, and the OCP of these copper alloys approaches that of the major constituent, Cu. Therefore, the OCP stabilizes at a much higher value when CE is terminated, compared with the result under the primary quiescence condition.

In the neutral and alkaline solutions, the cathodic process is oxygen reduction:

$$O_2+2H_2O+4e\rightarrow 4OH^{-} \quad (7)$$

In the neutral solution, a protective film, which is mainly composed of Cu_2O and Al_2O_3, can be rapidly generated on the NAB surface [39]. CE destructs this film and shifts the OCP of the NAB to a more negative value. However, active dissolution of the κ phases occurs for both the MAB and MB, and MB is subjected to dezincification corrosion. CE shifts the OCP of both the MAB and MB towards a more positive value as a result of the expedited mass transfer of the dissolved oxygen. In the solution of pH 12, passive films can be rapidly built on the NAB and MB under the quiescence condition, as evidenced by Figs. 2 and 3. Thus, CE decreases the OCP of these two materials as a result of the film destruction. However, CE shifts the OCP of the MAB to a more positive value, owing to the accelerated cathodic process and the absence of a protective passive film.

CE creates an increase of J_{corr} for each copper alloy, whether the anodic or cathodic process is accelerated. In the neutral and alkaline solutions, the three copper alloys possess similar J_{corr} under the CE condition (Table 3), because the electrochemical process is controlled by oxygen diffusion and the J_{corr} is decided by the dissolved oxygen content in the solution. The J_{corr} in the solution of pH 2 is much higher than that in other solutions for each copper alloy, owing to the active dissolution of the κ phases and the coexistence of hydrogen evolution and oxygen reduction in the cathodic process.

3.5 CE−corrosion synergy

As generally accepted, a synergistic effect exists between corrosion and mechanical attack. The CE−corrosion synergy (S) is composed of the corrosion-enhanced-CE (ΔE) and CE-enhanced-corrosion (ΔC). The following equation is widely used to evaluate the CE-corrosion synergy [19]:

$$T=E+C+S=E+\Delta E+(C+\Delta C) \quad (8)$$

where T and E represent the total mass loss rate of the materials in the corrosive solution and distilled water, respectively. The calculation methods of the pure corrosion rate (C) and the corrosion rate under the CE condition ($C+\Delta C$) have been stated in our previous research [40]. The mass loss rates induced by different components and their contribution to the cumulative CE mass loss rate are listed in Table 4.

For each copper alloy in each solution, the C/T value is very small, indicating that the pure corrosion has little effect on the CE damage. In the solution of pH 2, the S/T is the largest and even exceeds 60% for each material, and the $\Delta E/T$ is larger than the $\Delta C/T$. Among the three copper alloys, the MAB has the lowest E/T (25.38%) and the largest S/T (73.63%, $\Delta E/T$=46.97% and $\Delta C/T$=26.66%). The MB has the largest $\Delta E/T$ (53.36%). The $\Delta E/T$ and $\Delta C/T$ are pretty close for the NAB. In other solutions, the E/T is the largest for each copper alloy, demonstrating that mechanical attack is the dominant factor for the CE degradation. In the neutral solution, the MB has the largest E/T (88.27%), whereas the NAB has the largest S/T (38.97%) among the three materials. The $\Delta E/T$ is larger than the $\Delta C/T$ for each material, and

Table 4 Analysis results of CE−corrosion synergy in 3.5% NaCl solution with different pH values for copper alloys

Material	pH	Mass loss rate/(mg·cm^{-2}·h^{-1})					
		T	E (E/T)	C (C/T)	ΔE ($\Delta E/T$)	ΔC ($\Delta C/T$)	S (S/T)
MAB	2	4.7917	1.2160 (25.38%)	0.0472 (0.99%)	2.2509 (46.97%)	1.2776 (26.66%)	3.5285 (73.63%)
	6.8	1.7417	1.2160 (69.82%)	0.0106 (0.61%)	0.4047 (23.24%)	0.1104 (6.33%)	0.5151 (29.57%)
	12	1.3500	1.2160 (90.07%)	0.0172 (1.27%)	0.0061 (0.45%)	0.1107 (8.21%)	0.1168 (8.66%)
NAB	2	1.9667	0.7160 (36.41%)	0.0150 (0.76%)	0.6507 (33.09%)	0.5850 (29.74%)	1.2357 (62.83%)
	6.8	1.1833	0.7160 (60.51%)	0.0062 (0.52%)	0.3925 (33.17%)	0.0687 (5.80%)	0.4612 (38.97%)
	12	0.8833	0.7160 (81.06%)	0.0118 (1.34%)	0.0546 (6.18%)	0.1009 (11.42%)	0.1555 (17.60%)
MB	2	9.4833	3.0600 (32.27%)	0.0190 (0.20%)	5.0606 (53.36%)	1.3437 (14.17%)	6.4043 (67.53%)
	6.8	3.4667	3.0600 (88.27%)	0.0130 (0.37%)	0.2842 (8.20%)	0.1095 (3.16%)	0.3937 (11.36%)
	12	3.2500	3.0600 (94.15%)	0.0007 (0.02%)	0.0774 (2.38%)	0.1119 (3.45%)	0.1893 (5.83%)

the MAB and NAB have much larger $\Delta E/T$ values (23.24% for MAB and 33.17% for NAB) than the MB (8.2%). In the alkaline solution, the E/T is much higher than that in the neutral solution for each material. It reaches 81.06% for the NAB and even exceeds 90% for the MAB and MB. The $\Delta C/T$ is larger than the $\Delta E/T$, and it is about 8.20% for the MAB and 11.42% for the NAB. The NAB has the largest $\Delta E/T$, which is only 6.18%.

For each copper alloy, the dissolution of these κ phases creates many corrosion pits and holes on the surface in the solution of pH 2 (Figs. 6 and 7). This increases the surface roughness and remarkably weakens the mechanical properties. Therefore, a huge ΔE is induced. Besides, dezincification corrosion of the β phase further decreases the mechanical properties of the MB, and the β phase is severely eroded under the cavitation attack. Moreover, CE accelerates the oxygen transfer in the solution and results in ΔC for all the copper alloys. In the neutral solution, the preferential corrosion of the κ phases weakens the cohesion of α/κ phase boundary and thereby facilitates the detachment of these κ phases for both the MAB and MB. The dezincification corrosion of the β phase and the low mechanical properties (the hardness is about HV 124 for the MB and HV 175 for the NAB and MAB) give rise to the lowest CE resistance of the MB. The brittle fracture of the β phase and detachment of the large-sized rosette κ phases are responsible for the higher CE rate of the MAB, compared with the result of the NAB. The SPC of the lamellar α phase can promote the collapsing of the eutectoid microstructure in the NAB under the cavitation attack, and cavities are found at the eutectoid microstructure (Fig. 7(e)), as also previously reported [40,41]. In the solution of pH 12, each copper alloy undergoes much slighter corrosion damage (Figs. 6(c, f, i)), and thus the $\Delta E/T$ value is smaller. The mechanical attack is dominantly responsible for the CE damage. For the MB, the disappearance of dezincification corrosion also contributes to its high CE resistance in the alkaline solution. Moreover, corrosion products are found locally on the eroded surface of the MB after a CE duration of 5 h (Fig. 7(i)), and the chemical composition obtained by EDS is 26.79% O, 6.15% Al, 3.11% Mn, 16.71% Fe, 29.15% Cu, 17.53% Zn and 0.57% Cl. They can act as barriers to protect the substrate from violent mechanical attack.

4 Conclusions

(1) The SKPFM results indicate that the phase

nobility of the MAB and MB ranges from high to low as κ, β and α. For the NAB, the κ_{II} phase has the lowest nobility because it contains the largest Al and Fe contents.

(2) Each copper alloy exhibits different SPC behaviors when the pH value is changed. In the solution of pH 2, no protective films are built and the κ phase with low nobility undergoes preferential dissolution. In the neutral solution, the κ phases of the NAB are preserved because of the formation of Al_2O_3 film, but the κ phases of the MAB and MB are preferentially dissolved. Dezincification corrosion occurs at the β phase of the MB in both the acidic and neutral solutions. In the solution of pH 12, each copper alloy exhibits a passive behavior. Pitting corrosion mainly occurs at the κ phase of the MAB and MB, and the κ_{II} phase of the NAB. SKPFM results should be treated cautiously when corrosion product films are built on the copper alloys.

(3) The MDE ranges from high to low as MB, MAB and NAB in each solution. In the solution of pH 2, the MDE is the largest for each copper alloy, because the dissolution of the κ phases creates many corrosion pits on the surface and remarkably accelerates the CE damage. The CE−corrosion synergy contributes largely to the CE degradation. In other solutions, all the copper alloys exhibit a mechanical attack-dominated damage mechanism. Much slighter corrosion damage occurs in the solution of pH 12, the MDE is the lowest and the E/T exceeds 80% for each copper alloy.

(4) A negative OCP shift is induced by CE for the NAB in both the neutral and alkaline solutions and the MB in the alkaline solution, as a result of the destruction of the protective films, which are built under the quiescence condition. CE increases the corrosion current density for each material in each solution.

Acknowledgments

This research was financially supported by the Natural Science Foundation of Jiangsu Province, China (No. BK20191161), the Fundamental Research Funds for the Central Universities of China (No. B210202129), the National Natural Science Foundation of China (Nos. 51601058, 51879089), Changzhou Sci & Tech Program, China (No. CJ20210154) and Postgraduate Research and Innovation Project of Jiangsu Province, China (No. KYCX22_0599).

References

[1] TUTHILL A H. Guidelines for the use of copper alloys in seawater [J]. Materials Performance, 1987, 26: 12−22.

[2] SHARIFI E, RANJBAR K. Dezincification assisted cracking of yellow brass tubes in a heat exchanger [J]. Engineering Failure Analysis, 2022, 136: 106200.

[3] TANG Chi-hong, CHENG Fai-tsun, MAN Hau-chung. Effect of laser surface melting on the corrosion and cavitation erosion behaviors of a manganese−nickel−aluminium bronze [J]. Materials Science and Engineering A, 2004, 373: 195−203.

[4] YU Hong, ZHENG Yu-gui, YAO Zhi-ming. Cavitation erosion corrosion behaviour of manganese−nickel−aluminum bronze in comparison with manganese-brass [J]. Journal of Materials Science and Technology, 2009, 25: 758−766.

[5] CULPAN E A, ROSE G. Microstructural characterization of cast nickel aluminum bronze [J]. Journal of Materials Science, 1978, 13: 1647−1657.

[6] IQBAL J, HASAN F, AHMAD F. Characterization of phases in an as-cast copper−manganese−aluminum alloy [J]. Journal of Materials Science and Technology, 2006, 22: 779−784.

[7] CULPAN E A, ROSE G. Corrosion behaviour of cast nickel aluminium bronze in sea water [J]. British Corrosion Journal, 1979, 14: 160−166.

[8] LORIMER G W, HASAN F, IQBAL J, RIDLEY N. Observation of microstructure and corrosion behaviour of some aluminium bronzes [J]. British Corrosion Journal, 1986, 21: 244−248.

[9] ALHASHEM A, CACERES P G, RIAD W T, SHALABY H M. Cavitation corrosion behavior of cast nickel−aluminum bronze in seawater [J]. Corrosion, 1995, 51: 331−342.

[10] NEODO S, CARUGO D, WHARTON J A, STOKES K R. Electrochemical behaviour of nickel-aluminium bronze in chloride media: Influence of pH and benzotriazole [J]. Journal of Electroanalytical Chemistry, 2013, 695: 38−46.

[11] SONG Qi-ning, ZHENG Yu-gui, NI Ding-rui, MA Zong-yi. Studies of the nobility of phases using scanning Kelvin probe microscopy and its relationship to corrosion behaviour of Ni−Al bronze in chloride media [J]. Corrosion Science, 2015, 92: 95−103.

[12] WHARTON J A, STOKES K R. The influence of nickel−aluminium bronze microstructure and crevice solution on the initiation of crevice corrosion [J]. Electrochimica Acta, 2008, 53: 2463−2473.

[13] SONG Qi-ning, XU Nan, TONG Yao, HUANG Chen-ming, SUN Shou-yu, XU Chen-bo, BAO Ye-feng, JIANG Yong-feng, QIAO Yan-xin, ZHU Zhi-yuan, WANG Zheng-bin. Corrosion and cavitation erosion behaviours of cast nickel aluminium bronze in 3.5% NaCl solution with different sulphide concentrations [J]. Acta Metallurgica Sinica: English Letters, 2019, 32: 1470−1482.

[14] YUAN Shao-jun, PEHONEN S O. Surface characterization and corrosion behavior of 70/30 Cu−Ni alloy in pristine and sulfide-containing simulated seawater [J]. Corrosion Science, 2007, 49: 1276−1304.

[15] LV Yu-ting, GUO Jia-wei, ZHANG Guo-song, CAO

Lian-min, SUN Xue-yan, QIN Zhen-bo, XIA Da-hai. Insights into the selective phase corrosion of as cast NiAl bronze alloy: Effect of electrical properties of each phase's protective film [J]. Journal of Alloys and Compounds, 2022, 891: 162008.

[16] NAKHAIE D, DAVOODI A, IMANI A. The role of constituent phases on corrosion initiation of NiAl bronze in acidic media studied by SEM−EDS, AFM and SKPFM [J]. Corrosion Science, 2014, 80: 104−110.

[17] SONG Qi-ning, XU Nan, JIANG Xing, LIU Yue, TONG Yao, LI Jun-sen, BAO Ye-feng, QIAO Yan-xin. Effect of sulfide concentration on the corrosion and cavitation erosion behavior of a manganese−aluminum bronze in 3.5% NaCl solution [J]. Journal of Materials Engineering and Performance, 2019, 28: 4053−4064.

[18] PUNBURI P, TAREELAP N, SRISUKHUMBO-WORNCHAI N, EUARUKSAKUL C, YORDSRI V. Correlation between electron work functions of multiphase Cu−8Mn−8Al and de-alloying corrosion [J]. Applied Surface Science, 2018, 439: 1040−1046.

[19] WOOD R J K. Marine wear and tribocorrosion [J]. Wear, 2017, 376/377: 893−910.

[20] BASUMATARY J, WOOD R J K. The synergistic effects of cavitation erosion–corrosion in ship propeller materials [J]. Journal of Bio- and Tribo-Corrosion, 2015: 1−12.

[21] BASUMATARY J, WOOD R J K. Different methods of measuring synergy between cavitation erosion and corrosion for nickel aluminium bronze in 3.5% NaCl solution [J]. Tribology International, 2020, 147:104843.

[22] HALAS S, DURAKIEWICZ T. Work functions of elements expressed in terms of the Fermi energy and the density of free electrons [J]. Journal of Physics—Condensed Matter, 1998, 10: 10815−10826.

[23] ASTM G32—10. Standard test for cavitation erosion using vibratory apparatus [S]. 2010.

[24] SHI Zi-jie, WANG Zheng-bin, WANG Xiao-di, ZHANG Song, ZHENG Yu-gui. Effect of thermally induced B2 phase on the corrosion behavior of an Al0.3CoCrFeNi high entropy alloy [J]. Journal of Alloys and Compounds, 2022, 903: 163886.

[25] IANNUZZI M, VASANTH K L, FRANKEL G S. Unusual correlation between SKPFM and corrosion of nickel aluminum bronzes [J]. Journal of the Electrochemical Society, 2017, 164: C488−C497.

[26] DU Lin-lin, ZHANG Guo-teng, WEI Liang, XING Juan-juan, JIANG Ying, LI Qian, GU Hui. Inhomogeneous phases in Cu−Zn−Al−Fe−Mn and the micro-galvanic coupling in 3.5 wt.% NaCl solutions at different pH [J]. Corrosion Science, 2022, 195: 110005.

[27] CHEN Lin, CHEN Yan-jun, YANG Hui-sheng, SU Yan-jing, QIAO Li-jie. Study of the relationship between intergranular stress corrosion cracking and grain boundary characteristics in brass [J]. Electrochemistry Communications, 2021, 131: 107124.

[28] TRETHEWEY K R, HALEY T J, CLARK C C. Effect of ultrasonically induced cavitation on corrosion behaviour of a copper–manganese–aluminium alloy [J]. British Corrosion Journal, 1988, 23: 55−60.

[29] de SOUZA J S, de OLIVEIRA M C L, ANTUNES R A, da SILVA R A G. Effects of Sn, Gd, and Mn additions on the surface chemistry and electrochemical behavior of CuAl-based alloys in sodium chloride solution [J]. Applied Surface Science, 2022, 573: 151488.

[30] SONG Qi-ning, ZHANG Hao-nan, LI Hui-lin, HONG Hao, SUN Shou-yu, XU Nan, ZHANG Gen-yuan, BAO Ye-feng, QIAO Yan-xin. Corrosion and cavitation erosion behaviors of the manganese−aluminum−bronze cladding layer prepared by MIG in 3.5% NaCl solution [J]. Materials Today Communications, 2022, 31: 103566.

[31] SÜRY P, OSWALD H R. On the corrosion behaviour of individual phases present in aluminium bronzes [J]. Corrosion Science, 1972, 12: 77−90.

[32] ASGARI M, FORATIRAD H, GOLABADI M, KARIMI M, GHOLAMI M G. Investigation of the corrosion behavior of aluminum bronze alloy in alkaline environment [J]. Materials Science and Engineering Technology, 2021, 52: 511−519.

[33] KONG Deng-cheng, DONG Chao-fang, NI Xiao-qing, XU Ao-ni, HE Chang, XIAO Kui, LI Xiao-gang. Long-term polarisation and immersion for copper corrosion in high-level nuclear waste environment [J]. Materials and Corrosion, 2017, 68: 1070−1079.

[34] DINNAPPA R K, MAYANNA S M. The dezincification of brass and its inhibition in acidic chloride and sulphate solutions [J]. Corrosion Science, 1987, 27: 349−361.

[35] KAISER S, KAISER M S. A comparative study of chemical and physical properties of copper and copper alloys affected by acidic, alkaline and saline environments [J]. Journal of Electrochemical Science and Engineering, 2020, 10: 373−384.

[36] MORALES J, FERNANDEZ G T, ESPARZA P, GONZALEZ S, SALVAREZZA RC, ARVIA A J. A comparative study on the passivation and localized corrosion of α, β, and $\alpha + \beta$ brass in borate buffer solutions containing sodium chloride—I. Electrochemical data [J]. Corrosion Science, 1995, 37: 211−229.

[37] ZHENG Yu-gui, LUO Su-zhen, KE Wei. Effect of passivity on electrochemical corrosion behavior of alloys during cavitation in aqueous solutions [J]. Wear, 2007, 262: 1308−1314.

[38] KWORK C T, CHENG F T, MAN H C. Synergistic effect of cavitation erosion and corrosion of various engineering alloys in 3.5% NaCl solution [J]. Materials Science and Engineering A, 2000, 290: 145−154.

[39] SCHUSSLER A, EXNER H E. The corrosion of nickel-aluminum bronzes in seawater—I. Protective layer formation and the passivation mechanism [J]. Corrosion Science, 1993, 34: 1793−1802.

[40] SONG Qi-ning, TONG Yao, XU Nan, SUN Shou-yu, LI Hui-lin, BAO Ye-feng, JIANG Yong-feng, WANG Zheng-bin, QIAO Yan-xin. Synergistic effect between cavitation erosion and corrosion for various copper alloys in sulphide-containing 3.5% NaCl solutions [J]. Wear, 2020, 450−451: 203258.

[41] SONG Qi-ning, LI Hui-lin, ZHANG Hao-nan, HONG Hao, XU Nan, ZHANG Gen-yuan, BAO Ye-feng, QIAO Yan-xin. Correlation between microstructure and corrosion and cavitation erosion behaviors of nickel aluminum bronze [J]. Transactions of Nonferrous Metals Society of China, 2022, 32: 2948−2964.

不同 pH 值 3.5% NaCl 溶液中多种铜合金的选相腐蚀和空蚀行为

宋亓宁[1]，李慧琳[1]，许 楠[1]，蒋镇宇[1]，张根元[1]，包晔峰[1]，
蒋永锋[1]，赵立娟[1]，姬翠翠[1]，赵建华[1]，乔岩欣[2]

1. 河海大学 机电工程学院，常州 213022；
2. 江苏科技大学 材料科学与工程学院，镇江 212003

摘 要：采用扫描开尔文力显微镜(SKPFM)对镍铝青铜(NAB)、高锰铝青铜(MAB)及锰黄铜(MB)中不同相的稳定性进行表征，并对 3 种铜合金在不同 pH 值 3.5% NaCl 溶液中的选相腐蚀及空蚀行为进行研究。结果显示，在酸性溶液(pH 2)中，每种材料中稳定性最差的 κ 相均发生溶解。在中性溶液(pH 6.8)中，NAB 中富 Al 的 κ 相未发生腐蚀，而 MAB 和 MB 中富 Fe 的 κ 相发生溶解。在碱性溶液(pH 12)中，点蚀发生在 MAB 和 MB 的 κ 相以及 NAB 中的 κ_{II} 相上。在任一溶液中，耐空蚀性能顺序均为：NAB > MAB > MB。在酸性溶液中，选相腐蚀显著加重空蚀损伤，且腐蚀−空蚀交互作用是导致空蚀的主导因素；在其他溶液中，选相腐蚀较为轻微，3 种铜合金均表现出以力学损伤为主导的空蚀损伤机制。

关键词：铜合金；扫描开尔文力显微镜；选相腐蚀；空蚀；交互作用

(Edited by Bing YANG)